Temporary Nanoencapsulation of Human Intestinal Organoids Using Silk Ionomers

Brooke Wang[1], Onur Hasturk[1], Udathari Kumarasinghe[2], Sara Rudolph[1], Cristian Staii[2], Ying Chen[2]*, David L. Kaplan[2]*,

[1] Department of Biomedical Engineering, Tufts University, Medford, MA

[2] Department of Physics and Astronomy, Tufts University, Medford, MA

*Corresponding authors: ying.chen@tufts.edu, david.kaplan@tufts.edu.

Abstract

Human intestinal organoids (HIOs) are vital for modeling intestinal development, disease, and therapeutic tissue regeneration. However, their susceptibility to stress, immunological attack, and environmental fluctuations limits their utility in research and therapeutic applications. This study evaluated the effectiveness of temporary silk protein-based layer-by-layer (LbL) nanoencapsulation technique to enhance the viability and functions of HIOs against common biomedical stressors, without compromising their native functions. We assessed cell viability and differentiation capacity, finding that nanoencapsulation significantly improved HIO survival under the various environmental perturbations studied without compromising cellular functionality. Post-stress exposures, the encapsulated HIOs still successfully differentiated into essential intestinal cell types such as enterocytes, goblet cells, enteroendocrine cells, and Paneth cells. Moreover, the silk nanocoatings effectively protected against environmental stressors such as UV light exposure, protease degradation, antibody binding, and cytokine-induced inflammation. This nanoencapsulation technique shows promise for advancing HIO applications in disease modeling, drug testing, and potential transplantation therapies.

Keywords: intestinal organoids, cell encapsulation, silk ionomers, layer-by-layer assembly.

Introduction

Historically, biological research has predominantly relied on animal models, which cannot fully capture human-specific biological processes and diseases[1-3]. Recent advances in stem cell research have facilitated the development of organoids, often described as "mini organs". These organoids, comprising various cell types from the original organ, effectively replicate some of its fundamental functions[4-6]. Human intestinal organoids (HIOs) are especially noteworthy in this domain. HIOs can be derived from either stem cells or intestinal biopsies forming spherical clusters of cells encapsulated in an extracellular matrix (ECM) hydrogel. They are maintained in vitro by a cocktail of growth factors that prompt the cells to differentiate and self-organize into structures resembling the human intestine [7]. HIOs offer crucial insights into human intestinal diseases and serve as valuable complements to animal models, significantly enhancing our understanding of infectious diseases[8-11], genetic disorders[12,13], and cancers[14-16]. They also offer potential for gut disease treatment through both in vitro disease modeling and *in vivo* transplantation for tissue regeneration[17,18]. Despite their significant potential, the broader application of HIOs is constrained by several challenges. The primary issue is their inherent fragility and sensitivity. In both research and potential therapeutic contexts, external factors such as mechanical stress, immune system reactions, and environmental changes can significantly compromise their viability and functions. This reduction in reliability and robustness hampers their wider adoption in the field[19,20].

The burgeoning field of cell encapsulation has garnered significant interest in bioengineering and regenerative medicine, offering promising solutions for protecting mammalian cells from mechanical and biological stressors such as centrifugal[21], shear forces[22], and UV radiation[23], as well as biological threats like osmotic pressure changes[24], and temperature fluctuations[25]. This technology is particularly critical in tissue regeneration and transplantation therapy, where these coatings can reduce transplantation rejection by shielding cells from immunogenic responses like proteolytic enzymes[26] and cytokine tagging[27]. In cellular encapsulation, two main techniques are used: microencapsulation and nanoencapsulation. Microencapsulation typically involves encapsulating cells in a polymeric matrix forming microspheres or microbeads at the micrometer scale[28]. However, due to the nature of the polymers used in microencapsulation, such as alginate and poly-L-lysine (PLL), significant limitations are imposed in the uniformity[29], tunability[30] and stability[31] of the microspheres. In contrast, nanoencapsulation coats cells at the nanometer scale using a layer-by-layer (LbL) method that deposits polymers electrostatically onto cell membranes[32,33]. Nanoencapsulation has become preferred over microencapsulation due to improved reproducibility, uniformity, and lower cytotoxicity[34,35] as well as enhanced control over the nanoshell properties, such as duration, permeability, degradability, and functionality[36,37]. This adaptability enables the design of nanocoatings tailored for specific applications like transplantation, optimizing properties such as biocompatibility, cell proliferation, and immunocloaking[33].

Biocompatible materials are essential for cell viability during encapsulation applications[38]. While traditional polymers, including poly-L-lysine/hyaluronic acid[39], gelatin[40,41], collagen[36], and chitosan/alginate[33,42,43], have been used, silk fibroin (SF) protein derived from *Bombyx mori* silkworms offers exciting possibilities. SF self-assembles into materials with crystalline β-sheet structures, providing significant mechanical strength and biodegradability - ideal for cell coating applications [22,44,45]. The tunability of SF [46,47], through adjustments in molecular weight, chemical

modifications, and β-sheet density, enables the generation of tailored and temporary nanocoatings for diverse biomedical needs, establishing SF as a transformative material in cell encapsulation and regenerative medicine.

Previous research on nanoencapsulation has predominantly centered on the coating of single-cells from both mammalian and bacterial sources, including bacteria[48], yeast[49], human erythrocytes[50], fibroblasts[44], neural stem cells[41], immune cells[45] and human mesenchymal stem cells (MSCs)[22]. These studies have achieved varying degrees of success in protecting cell viability post-encapsulation. However, the application of nanoencapsulation techniques to larger cell aggregates and 3D multicellular structures, like HIOs, remains less explored.

In this present study, we build on our prior research[45] to investigate the deposition of functionalized silk on the surface of HIOs using the LbL technique. The approach involves alternately coating the HIOs with aminated (positively charged) and carboxylated (negatively charged) silk layers to generate a temporary protective shell. Our aims were to evaluate the effectiveness and duration of silk encapsulation, to assess the viability and differentiation of the HIOs following encapsulation, and to determine the protective capabilities of these silk nanoshells against environmental stressors.

Methods and Materials

Preparation of aminated and carboxylated silk

Silk fibroin (named silk thereafter) solutions were prepared from *Bombyx mori* silkworm cocoons as previously described[46]. In short, silk cocoons were boiled for 60 and 120 mins in 0.02 M Na_2CO_3, stirring occasionally. After drying, the silk was dissolved in 9.3 M LiBr and dialyzed against deionized water for 72 hours. The resulting silk solution was centrifuged 2x for 20 mins at 9,000 rpm at 4℃. A representative sample from the resulting solution was dehydrated in a 60℃ oven overnight. The weight of the dehydrated sample was compared to that of the original aqueous solution weight to calculate silk concentration in solution (w/w). Functionalization of silk was performed in accordance with the procedure reported by our lab [44]. Briefly, for the carboxylation of the tyrosine groups, a diazonium salt solution was prepared by mixing 34 mg of 4-aminobenzoic acid with a cooled 1.25 mL of acetonitrile solution, followed by the addition of 625 µL cooled $NaNO_2$ solution and 625 µL p-toluene sulfonic acid. The solution was then vortexed briefly and incubated on an ice bath for 15 mins. Then 15 mL of the diazonium salt solution obtained as described above was mixed with 50 mL of 4% w/v 120 min boiled aqueous silk solution prepared in 0.1 M sodium carbonate buffer (pH 9.0). The silk solution was incubated on ice for 20 mins and then loaded into 3.5 kDa cutoff dialysis tubing. The carboxylated silk was dialyzed against DI water for 4 days with 2 water changes per day, centrifuged 2x at 9,000 rpm at 4℃ for 20 mins, flash frozen in liquid nitrogen, and lyophilized until dry. The samples were stored at –20℃ until further use. For the preparation of aminated silk, carbodiimide-coupling of ethylenediamine dihydrochloride (EDA) was performed. Briefly, a 2% w/v 60- mins boiled silk was reacted with EDA dihydrochloride at a concentration of 1.5 g per 1 g silk. This was performed in a 0.05 M 2-(N-morpholino)ethanesulfonic acid (MES) buffer (pH 6) in the presence of EDC (850 mg per 1 g silk) and N-Hydroxysuccinimide (NHS) (275 mg per 1 g silk) and reacted for 18 hours at room temperature. The solution was then loaded into 3.5 kDa cutoff dialysis tubing and dialyzed against deionized water for 4 days totaling 8 water changes. The silk solution was centrifuged twice at 9,000 rpm at 4℃ to remove any debris, flash

frozen in liquid nitrogen, and lyophilized until dry. The samples were stored at –20℃ until further use.

Fluorescein Isothiocyanate (FITC) labeling of aminated silk

In order to visualize silk deposition on the HIOs, aminated silk was fluorescently tagged using FITC as previously described[44]. Briefly, FITC (10 mg/mL) dissolved in DMSO was diluted 4 times with DI water. 10 mL of 5 mg/mL aminated silk dissolved in 0.1 M carbonate buffer (pH 9.0) was prepared and 100 µL of the FITC added and the solution was stirred for 1 hour at room temperature. The solution was then loaded into 3.5 kDa cutoff dialysis tubing and dialyzed against DI water for 3 days totaling 6 water changes. The silk solution was centrifuged 2x at 9,000 rpm at 4℃ for 20 mins to remove any debris, flash frozen in liquid nitrogen, and lyophilized until dry. The samples were stored at –20℃ until further use.

Maintenance of human intestinal HIOs

Human intestinal organoids, isolated from tissue biopsies of the human ileum (Baylor College of Medicine-Texas Medical Center Digestive Diseases Center Enteroid Core) were cultured according to previously established methods[51]. Briefly, HIOs were thawed under cool, running water and resuspended in complete media growth factor negative (CMGF–) (Advanced DMEM/F12 (AdvDMEM) (Invitrogen, Carlsbad, CA, USA), 10 mM HEPES buffer (Invitrogen), 1x GlutaMax (Gibco, Waltham, MA, USA), and 10,000 U/mL Penicillin-Streptomycin (Thermo Fisher, Waltham, MA, USA)) HIOs were centrifuged at 222 x g for 5 mins at 4 ℃ then resuspended in Matrigel (30 µL/well, Corning, Corning, NY, USA) droplets in a 24-well Nunclon Delta Surface plate (Thermo Fisher). The cells were incubated at 37℃ for 10 mins via the hang-drop method then fed with conditioned Wnt/R-spondin/Noggin (CWRN) growth medium (15% Advanced DMEM/F12 (Invitrogen) and 50% L-WRN conditioned media produced from ATCC CRL-3276 cells (Manassas, VA, USA) supplemented with 10 mM HEPES buffer (Invitrogen), 1x GlutaMax (Gibco), 2x B27 (Gibco), 1x N2 (Gibco), 10 mM Nicotinamide (Sigma-Aldrich, St. Louis, MO, USA), 500 nM N-Acetyl-Cysteine (Sigma-Aldrich), 500 nM A 83-01 (Sigma-Aldrich), 10 µm SB202190 (Sigma-Aldrich), 50 µm/mL epidermal growth factor (Peprotech, Cranbury, NJ, USA), 1:1000 Primocin (Invitrogen), and 10 nM gastrin I (Sigma-Aldrich). Additionally, 10 µM of Y-27632 (Sigma-Aldrich) was added to the complete growth media during the 1st passage. Enteroids were incubated at 37 ℃ (95% O_2/5% CO_2), media was changed every other day, and cells were passed every 5-7 days or until ~80% confluency (determined by light microscopy). HIOs were passaged in a 1:3 or 1:4 ratio based on an established protocol of mechanoenzymatic degredation from Matrigel using 1x TrypLE (Gibco).

Nanoencapsulation of human intestinal HIOs

A stock solution of aminated and carboxylated silk was prepared at a concentration of 2 mg/mL by dissolving the functionalized silk in an HD50 solution prepared with 40 mM HEPES buffer supplemented with 50 mg/mL of dextrose, and 50 mM NaCl (pH 7.4) in DI water supplemented by 0.1% bovine serum albumin (BSA) (Thermo Fisher). The solutions were sterile filtered (0.22 µm pore size, Sartorius) and kept on ice during the encapsulation. Enteroids were recovered

using 500 µL of 1x cell recovery solution (Corning) per well and incubated on ice for 30 mins then centrifugation at 180 x g at 4℃ for 5 mins. The cells were collected using wide-gauge tips and were thoroughly washed with 1 mL of HD50 and centrifuged at 180 x g at 4℃ for 5 mins. For the deposition of the first layer, 1 mL of the aminated silk solution was gently pipetted with the enteroids using wide-gauge tips then centrifuged at 180 x g at 4℃ for 5 mins. The supernatant was then aspirated and the cells washed using 1 mL of blank HD50 solution then the process was repeated for carboxylated silk. The alternating solutions were deposited onto the enteroids with blank buffer washes in between until either 3 or 5 bilayers was achieved.

Cell viability and propagation post-encapsulation

Cell viability was determined using a live-dead assay kit (Invitrogen) following the manufacturer's instructions 2 hours after encapsulation of HIOs with non-FITC labelled silk. Cells were imaged with a BZ-X700 Fluorescence Microscope (Keyence Corp., Itasca, IL, USA) with 494 nm/517 nm (Ex/Em) and 517 nm/617 nm (Ex/Em) filters. Live cells were detected by green signals while dead cells were detected by red signals. Cell proliferation was determined using an Alamar Blue reagent (Thermo Fisher) according to the manufacturer’s protocol at timepoints 0, 3, 5, and 7 days post-encapsulation with non-FITC silk and re-plating in Matrigel. Briefly, a 10% AlamarBlue (v/v) solution was prepared with the HIO culture medium and 300 µL of the solution was added to each well and was incubated at 37℃ for 2 hours. Fluorescence was read using a microplate reader (Molecular Devices, San Jose, CA, USA) at 530–560 nm/590 nm (Ex/Em).

Confocal laser scanning microscopy

Encapsulated HIOs were prepared with FITC-labelled aminated silk for post-encapsulation visualization using a TCS SP8 microscope from Leica Microsystems (Wetzlar, Germany) at 488 nm/500-540 nm (Ex/Em).

Scanning electron microscopy

After coating, HIOs were plated on 8.0 µm pore size translucent PET membrane inserts (Millipore Sigma, Burlington, MA, USA) and washed 2x with UltraPure DNase/RNase-Free Distilled Water (Thermo Fisher). A 1% glutaraldehyde fixing solution was prepared in UltraPure water and 300 µL of the fixing solution was added to each transwell and incubated at RT for 1 hour. Each transwell was washed using cold UltraPure water 5x on ice. Dehydration was performed using a graded ethanol series (30%, 50%, 70%, 90%, 100%) and hexamethyldisilazane (HMDS) was added to the transwells at the critical drying point. Samples were left overnight in a chemical hood after addition of HMDS and evaporated before SEM imaging (Zeiss EVO MA10, Germany).

Atomic force microscopy

Non-coated and coated HIOs plated on poly D-lysine (PDL) coated 8.0 µm pore size translucent PET membrane inserts (Millipore Sigma) and imaged using an Asylum Research MFP-3D-Bio

AFM (Asylum Research, Santa Barbara, CA, USA) with NanoWorld Pyrex-Nitride triangular (PNP-TR) AFM probes (Asylum Research) possessing a force constant of 0.08 N/m. 4x4 maps of individual force vs. indentation curves were acquired on an area of 400 μm^2 of the HIOs surface at multiple locations as HIOs were too large to capture a whole aggregate. The resulting force vs. indentation curves were used to mathematically determine the elastic modulus for each measurement.

Cell seeding to form monolayers

After encapsulation, HIOs were collected and dissociated to form monolayers. Briefly, a 96-well plate was collagen coated with 200 µL of a diluted collagen type I (First Link, UK) solution incubated overnight at 4°C. DPBS was removed from the settled collagen coating then each well was rinsed 3 x 200 µL DPBS. The collagen coat was airdry in the biohood with the lid slightly ajar for at least 10 minutes. Encapsulated cells were collected in a 15 mL conical tube and 0.5 mL of 0.05% Trypsin was added to each tube then incubated for 4 mins in a warm water bath. To neutralize the trypsin, 0.5 mL of 10% FBS in complete media without growth factors (CMGF–)s was added to each tube. Using a P1000 pipette, the cells were pipetted up and down 10-20x to mechanically break the HIOs into single-cells and proper dissociated was checked periodically under a light microscope. The dissociated cells were passed through a 40 µm cell strainer into a 50 mL conical tube and centrifuged for 5 min at 290 x g at RT. Cells were then resuspend in CWRN medium supplemented with 2 µL/mL CWRN of Y-27632 and media was refreshed every other day until 100% confluency was reached. After confluency, cells were fed with standard differentiation media (CMGF–, 5% Noggin, 1× B27, 1× N2, 1 mM N-acetylcysteine, 50 ng/mL epidermal growth factor, 10 nM gastrin I, and 500 nM A 83-01) for 3-5 days or until fingerprint morphology was observed within the monolayers.

Immunostaining

HIOs were immunostained either as monolayers in a 96-well collagen coated plate or as whole HIOs using an 8.0 µm pore size translucent PET membrane inserts (Millipore Sigma). Cells were fixed using 4% paraformaldehyde (PFA) for 10 minutes, rinsed 3x with DPBS, then permeabilized with 0.25% Triton 100X in a 1% BSA solution diluted in DPBS for 10 minutes at RT. Following a DPBS wash, cells were blocked for 30 minutes with a 3% BSA solution diluted in DPBS. Subsequently, cells were stained with ZO-1 (Invitrogen) and 4′,6-diamidino-2-phenylindole (DAPI) simultaneously for 3 hours before a final wash and imaging with a fluorescent microscope.

Real-time Quantitative Polymerase Chain Reaction (RT-qPCR)

Potential cellular differences due to nanoencapsulation at the transcript level was determined via RT-qPCR performed according to the manufacturer's protocol (Thermo Fisher). Briefly, 150 µL of buffer RLT was added to each well containing monolayers and scraped with a P1000 pipette tip. Lysed cells were homogenized then transferred to a spin column and spun 1x with 700 µL buffer RW1, and 2x with 500 µL buffer RPE. Resulting mRNA was confirmed to have an RNA concentration of ≥34 ng/µL via NanoDrop Microvolume Spectrophotometer (Thermo Fisher).

cDNA reverse transcription was performed according to the manufacturer's protocol in which 10 µL of 2x reverse transcription master mix was added to 0.2 mL PCR tubes (USA Scientific, Ocala, FL, USA) followed by 10 µL of 1 µg/reaction mRNA sample and contents were mixed. Tubes were briefly centrifuged and loaded into the thermal cycler (MJ Research, Saint-Bruno-de-Montarville, Canada). Finally, PCR reactions were prepared following the manufacturer's protocol with each well of a 96-well optical plate (BioRad, Hercules, CA, USA) containing 1x Yellow Sample Buffer, 1x PowerTrack SYBR Green Master Mix, 400 nM of forward and reverse primers (purchased from https://www.realtimeprimers.com/) .0.6 ng/mL of cDNA, and 6.5 µL of nuclease-free water. The optical plate was sealed with an adhesive cover and briefly centrifuged before loading into the real-time PCR thermocycler (BioRad).

UV functional test

After encapsulation, HIOs were suspended in conditioned media in a 6-well plate and placed approximately 10 cm under an 8 W UVP UVLMS-38 UV lamp (Analytik Jena AG, Thuringia, Germany) with a wavelength of 254 nm in a biohood for 30 minutes based on the procedure we previously reported[44]. Subsequently, a Caspase 3/7 assay was performed according to the manufacturer's protocol (Promega, Madison, WI, USA). Caspase-Glo 3/7 reagent was prepared by mixing Caspase-Glo Buffer with Caspase-Glo 3/7 Substrate. Equal volumes of Caspase-Glo 3/7 reagent and cells were added to a white-walled 96-well plate (Thermo Fisher) then evaluated using a luminometer plate reader (BioTek, Winooski, VT, USA). UV treated cells were additionally stained using a live-dead assay kit (Invitrogen) to determine cell viability as previously described.

TNF- α functional test

Tumor necrosis factor alpha (TNF- α) functional testing was performed based on the procedure previously outlined [44]. Following encapsulation, cells were replated in Matrigel and incubated for 72 hours in conditioned media supplemented by 100 ng/mL of (TNF-α) (Peprotech, NJ, USA). After 72 hours, cells mechanoenzymatically released from Matrigel and cellular apoptosis levels were evaluated using a Caspase 3/7 assay as previously described.

Trypsin functional test

Encapsulated HIOs were incubated in a 0.05% trypsin solution at 37°C for 10 minutes with occasional pipetting. Trypsin solution was neutralized with equal volume conditioned media solution supplemented by 10% FBS then centrifuged at 222 x g for 5 minutes. Cells were then replated in Matrigel, and cell viability was evaluated using a live-dead assay (Invitrogen) as previously described.

Statistical analysis

All calculations were performed using GraphPad Prism (GraphPad Software V10.2.3, La Jolla, CA) with data expressed as mean ± standard deviation. One-way analysis of variance (ANOVA) with Tukey's post hoc multiple comparison test were conducted after normality and homogeneity of variance assumptions were checked to determine statistical significance (*$p \leqslant 0.05$, **$p \leqslant 0.01$, ***$p \leqslant 0.001$, ****$p \leqslant 0.0001$).

Results and Discussion

Silk encapsulation efficacy and silk deposition on HIO surface

Previous studies have shown the successful encapsulation of single cells with SF [44,45,49]; however, encapsulation of larger cell aggregates, such as HIOs has yet to be explored. This study aimed to establish the feasibility of encapsulating HIOs using the LbL technique. The LbL technique was executed by alternately suspending HIOs in solutions of positively charged aminated silk fibroin (SF-EDA) and negatively charged carboxylated silk fibroin (SF(Y)COOH) (Fig. 1A). A 'bilayer' was defined as one positive and one negative layer. Positively charged aminated silk was applied as the initial layer for coating the surface of HIOs, followed by a layer of negatively charged carboxylated silk. This sequence is essential due to the inherently negative charge on HIO cell surfaces, which allows the positively charged aminated silk to adhere effectively through ionic interactions [52]. The first aminated silk layer forms a temporary, self-adherent coating on the cell surface without requiring secondary linking mechanisms. This ionic bonding creates a reversible attachment, enabling potential removal or disruption of the coating under mechanical or ionic forces, thus maintaining the adaptability of the HIO surface for experimental purposes. For this study, coatings of both 3 and 5 bilayers were used. The choice of 3 bilayers was based on previous work by our lab, which demonstrated successful silk deposition without affecting cell viability [44,53]. 2 additional bilayers (5-bilayers) were also tested in order to test the effects of manipulation the physical properties of the coating such as stiffness. Although cationic polymers, like SF-EDA, can be cytotoxic due to membrane destabilization [37,54], modifications to charge density, molecular weight, and cation concentration previously studied by the lab have significantly enhanced cell viability and biocompatibility of these biomaterials [44]. As previously reported, the yields for SF-EDA and SF(Y)COOH were 88.1% and 29.5%, respectively[44], and consequently, HIO encapsulation was carried out under these optimized conditions.

To visualize the silk coating on the cell surface, samples of SF-EDA were labelled with FITC (SF-FITC). Confocal microscopy confirmed the presence of SF-FITC at a concentration of 2 mg/mL around the entire surface of the coated HIOs (Fig. 1B-D). Similarly, fluorescence microscopy revealed a distinct green fluorescent ring around the samples after 3 and 5-bilayers of coating, indicating successful deposition and assembly of labeled silk on the HIO surfaces (Fig. 1E-G). The fluorescence signal was predominantly localized to the outermost surface of the HIOs, with no evident membrane damage or endocytosis. Additionally, SF-FITC signals on the outer surface of HIOs persisted for 48 hours, with degradation of the coating observed afterward (data not shown). Previous findings from our lab [44,45] and other studies[37,41,55] reported similar coating durations, typically between 24 and 48 hours. The release of the coating by 48 hours highlights the temporary nature of the silk coating. The silk bilayer construct of the same conditions was measured via zeta potential measurements to track successful layer deposition and time-depend dissolution has been previously reported by our lab [44].

To further validate the presence of the coating layer and assess surface topography alterations following encapsulation, uncoated and coated HIOs were imaged using SEM. SEM images of the uncoated HIOs exhibited typical HIO morphology, characterized by a spheroid shape and a rough surface texture (Fig. 1H). In contrast, the 'roughness' observed in uncoated HIOs was masked in the coated samples, suggesting successful deposition of silk on the HIO surfaces (Fig. 1I). Higher magnification images displayed silk ionomers forming a filamentous structure over the HIO surface, confirming the presence of silk encapsulation (Fig. 1J). The masking of cell

surface topological features via encapsulation has been observed by other studies on single cells, and corroborate the results demonstrated on HIOs[37,39,45,56].

HIO viability and metabolic activity following silk encapsulation.

To assess the effects of silk nanocoating and the encapsulation process on cell viability, live-dead staining was conducted immediately after coating, and AlamarBlue proliferation assays were performed over a seven-day period following coating.

Uncoated, control HIOs exhibited a mixture of live (green fluorescence signal) and dead (red fluorescence signal) cells, indicative of normal cell cycles in HIOs. The red staining signal was predominantly visible at the HIO center, while the green live stain encircled the necrotic core (Fig. 2A). A similar live and dead staining pattern was observed in the 3 and 5-bilayered coated groups (Fig. 2B, C). Quantitative analysis of cell viability, determined by the ratio of live cells to the total cell count within the culture showed that the quantity of living cells remained relatively consistent across the control, 3-bilayer, and 5-bilayer groups, with live viability ratios of 0.581±0.02, 0.633±0.01, and 0.580±0.01, respectively (Fig. 2D). The dead ratios were 0.412±0.02, 0.367±0.01, and 0.420±0.01 between the control, 3-bilayer, and 5-bilayer coated cells, respectively (Fig. 2E). The silk encapsulation, whether applied as a 3 or 5-bilayer coating, did not significantly affect the overall cell viability of the HIOs. Studies with single-cells typically report cell viability around 80% with various coatings[39,41,44,57]. The observed lower cell viability in HIO encapsulation is likely due to the inherent presence of a necrotic core, contributing to a higher proportion of dead cells, even in the control conditions. This distribution of dead cells in the HIO center is expected, as HIOs shed apoptotic cells from villi tips into the luminal center[58,59].

AlamarBlue assays showed a general upwards trend in the proliferation of both control and coated cells over 7 days (Fig. 2F). The similar proliferation rates between the two groups suggest the biocompatibility of the silk coating for short-term encapsulations. This observation contrasts with single-cell studies that reported impaired proliferation following nanocoating [22,56,60]. It has been proposed that multicellular aggregates, such as HIOs, enhance cell survival under coated conditions due to increased cell-cell interactions, compared to single cells [36,43].

Previous studies on single cells have typically limited coating to 3 bilayers because of significant viability reductions, likely due to cation-membrane charge interference [39,45]. However, our findings indicate that the multicellular structure of HIOs tolerates more coating bilayers with minimal impact on viability and proliferation (Fig 2D, F). The silk material used for coating may aid in increased cell viability by providing a selective structure that allows essential nutrients and growth factors to reach the cells[61] while inhibiting larger, potentially damaging molecules such as proteases, antibodies, and cytokines (Fig. 4C, D; Fig. 5). Additionally, the silk coating's permeability, as shown by other researchers, can be adjusted based on environmental factors like pH to be more or less porous, and therefore selective, in order to enhance cell viability in different environments[62].

HIO differentiation potential following the coating.

HIOs, which are 3D spheroids populated with stem cells, can be sustained long-term in a laboratory setting. These organoids can differentiate into various epithelial cell types found in the human intestine, including enterocytes, Goblet cells, enteroendocrine cells, and Paneth cells [63]. This ability allows HIOs to closely mimic the cellular composition of the actual intestine, making them an excellent model for biological and biomedical research. Typically, HIOs are

cultivated as 3D spheroids in Matrigel, featuring a micro-scaled enclosed lumen with apical cell surfaces oriented inward and basal surfaces exposed to the Matrigel. However, accessing the lumen of HIOs for luminal stimulation or bacterial infections has been challenging, which has limited their use in modeling intestinal tissues and diseases as whole spheroids [64]. To address this limitation, a method to convert the organoids into monolayers has been utilized, usually using a mechano-enzymatic dissociation that separates the spheroids into singlets or doublets. These cells are then seeded to form confluent monolayers on designated culture platforms. Once differentiated, these monolayers comprise all major intestinal epithelial cell types, significantly enhancing their utility for further applications [65]. These monolayers have proven to be instrumental in facilitating mechanistic studies on various bacterial and viral infections [66,67].

In our study, we aimed to investigate how silk coatings influence the differentiation and fate of organoids. HIOs were coated with silk ionomers using a LbL technique and encapsulated with either 3 or 5 bilayers of silk. Once encapsulated, the organoids were dissociated and plated onto collagen-coated wells to form monolayers. Following differentiation, two types of analyses were performed. First, cells were fixed and immunostained with Zonula ocludens (ZO-1), a tight-junction protein that indicates the formation of a barrier by differentiated intestinal epithelial cells. Second, mRNA was extracted from the monolayers to assess the expression levels of marker genes associated with differentiation.

Fluorescence images of the ZO-1/DAPI staining (Fig. 3A-C) showed that confluent monolayers were successfully formed under all three conditions, control, 3-bilayers, and 5-bilayers, and exhibited no morphological differences among groups. ZO-1 staining displayed the characteristic 'chicken-wire' pattern in all groups, indicating successful differentiation with no observable impact from the silk layers (Fig. 3A-C).

To further explore potential cellular differences at the transcript level resulting from the nanoencapsulation process, real-time quantitative polymerase chain reaction (RT-qPCR) was performed on six key organoid differentiation markers: sucrose-isomaltase (SI, enterocyte marker), mucin-2 (Muc2,Goblet cell marker), Lysozyme (Paneth cell marker), Chromogranin A (ChgA, enteroendocrine cell marker), and leucine-rich-repeat-containing G-protein-coupled receptor 5 (Lgr-5, stem cell marker). This analysis was conducted after the organoids were coated and plated into monolayers as previously described. The RT-qPCR results showed that post-differentiation, all organoid-derived epithelial monolayers, whether non-coated or coated with 3 or 5 bilayers of silk, expressed the marker genes corresponding to their respective cell types, confirming successful differentiation (Figure 3D). Notably, the expression level of Lgr-5, an intestinal stem cell marker, was extremely low, which further supports the completion of differentiation. Additionally, there were no significant differences in the expression levels of differentiation markers between the control, 3-bilayer, and 5-bilayer groups, indicating that the silk coating did not adversely affect cellular differentiation (Figure 3D). These findings align with previous encapsulation studies using stems cells, which also reported no major impact of nanocoating on cell differentiation and functionality in both single neural stem cells coated with alginate[41] and MSCs coated with collagen type I/hyaluronic acid[68].

The “passive shells” used in this study, designed to minimally impact cell behavior, can be transformed into “active coatings” by incorporating growth factors, antibodies, or other polymers to purposefully modify the cell surface or their external environments [38,69,70]. For example, grafting laminin-derived peptides onto poly(l-lysine) and poly(l-glutamic) acid LbL films influenced the differentiation of C2C12 myoblasts for use in muscle regeneration therapies and

cell amplification for transplantation [71]. Additionally, incorporating polymers like polyethylene glycol (PEG) into silk nanocoatings can mask antigens on cell surfaces, enhancing the success of cell transplantation [72].

Functional capabilities of silk encapsulation in protecting intestinal HIOs against various environmental stressors

The protective functions of the silk nanocoating on intestinal organoids when exposed to a range of stressors relevant to biomedical applications, including UV light, protease degradation, antibodies, and cytokines was assessed. The goal was to demonstrate the efficacy of silk nanocoatings in enhancing organoid stability and durability in harsh environments, potentially paving the way for improved therapeutic and research applications.

UV Light Exposure

We selected UV-C radiation exposure for HIOs due to its established antimicrobial properties and frequent use in sterilizing process involved in tissue cultures, 3D prints, and transplantable materials [73]. The effectiveness of UV-C radiation stems from its ability to cause irreversible genetic damage to microorganisms, making it essential for sterilization[74]. However, its use in biomedical and regenerative medicine requires minimizing damage to mammalian cells. To assess its impact, we evaluated the response of silk nanocoated HIOs to UV-C radiation, focusing on viability and structural integrity, which is crucial for both laboratory and clinical settings. HIOs with silk nanocoatings were exposed to 254 nm UV-C light for 30 minutes. Cell apoptosis was then quantified using a Caspase 3/7 assay, which measures enzyme activity crucial in apoptosis. The results showed that nanocoatings provided significant protection against UV-C damage, with reduced apoptosis in 5-bilayer coated HIOs (17,556±5,538 cd/m^2) compared to the control (52,953±18,110 cd/m^2), and 3-bilayer groups (48,589±19,052 cd/m^2) (Fig. 4A). Statistical analysis revealed significant differences between the control and the 5-bilayer samples, and between the 3-bilayer and 5-bilayer samples (Tukey's HSD, $p<0.05$). Live-dead staining further confirmed a higher survival rate in the 3- and 5-bilayer groups compared to uncoated controls (Fig. 4A). The high tyrosine content of silk likely contributes to the coating's UV absorption properties as the aromatic side chains in tyrosine absorbs in the UV-C wavelength region[75]. Previous studies similarly showed significant increases in single cell viability after exposure to UV radiation when coated with inorganic mineral and metal-based nanoshells or hydrogels, though to our best knowledge, this study is the first to demonstrate the use of silk nanoshells in protecting large cell aggregates from UV-C-induced damage [23,76,77].

Resistance to Protease Degradation

In vivo, the gastrointestinal tract encounters a mix of endogenous and exogenous proteases, posing a significant challenge for cells, especially during transplantation[78,79]. Similarly, intestinal organoids are highly susceptible to enzymatic digestion during *in vitro* procedures such as passaging and monolayer generation. To evaluate the protective efficacy of the silk nanocoating against this proteolytic environment, we immersed HIOs in a 0.05% trypsin solution. This experiment served as a proof of concept to demonstrate the silk nanocoating's ability to shield cells from protease degradation. We then assessed cell viability to gauge the immediate protective effects of the nanocoating against protease-induced damage. Viability was evaluated through live-dead staining post-treatment and subsequent quantification revealed statistically

significant improvements in viability of coated HIOs compared to the uncoated control group (Fig. 4C, D). The live cell to total cell ratio of control HIOs was determined to be 0.633±0.03 while 3-bilayer and 5-bilayer live ratios were 0.774±0.05 and 0.799±0.06, respectively. Interestingly, there was no significant difference in viability between the 3-bilayer and 5-bilayer groups (Tukey's HSD, $p = 0.46$), suggesting that even a 3-bilayer coating provides significant protection against protease-induced damage. Prior encapsulation of yeast cells (*Saccharomyces cerevisiae*)[80] and human mesenchymal stem cells[81] indicated similar results with protection of encapsulated cells against proteolytic enzymes. Serine proteases are one of the largest families in the human proteome and are released by activated leukocytes during processes such as transplantation[82]. Additionally, recent studies have highlighted the role of proteases in activating specific protease-activated receptors (PARs) that significantly influence cellular processes such as apoptosis[83]. Therefore, inhibiting protease interactions with vulnerable cells, such as HIOs, via silk nanocoatings can enhance the viability and survival of HIOs after transplantation.

Antibody Binding Inhibition

To further evaluate the protective capabilities of silk nanocoatings, their effectiveness against macromolecular interactions, specifically antibody binding, was tested. This functionality is critical for understanding the coating's potential in clinical and research settings where immune reactions via antibody binding can affect cell viability post-transplantation[84]. Whole-HIO immunostaining was performed and evaluated to determine the effectiveness of silk nanocoating in blocking antibody access to surface proteins. Zonula occludens-1 (ZO-1), a tight junction protein that typically forms a continuous lining around cell borders in healthy epithelial layers[85], was chosen as a marker.

In uncoated controls, clear ZO-1 staining depicted robust antibody interaction with surface antigens, displaying the typical "chicken-wire" morphology, indicative of uninhibited access (Fig. 5A, B). Conversely, silk-coated samples showed markedly reduced ZO-1 staining, lacking the distinct pattern, suggesting the nanocoatings hindered antibody binding (Fig. 5C-F). This muted and disrupted fluorescence indicates effective blocking of antibodies by the nanocoating, reinforcing its role as a protective barrier - a function similarly noted in coated human pancreatic islets, where it prevented antibody recognition [86]. This protective effect was further supported by DAPI staining of the nuclei in the same samples. DAPI, being a smaller immunostaining molecule than typical antibodies, also showed less pervasive staining in the coated HIOs (Fig. 5C, E). Thus, the coating not only prevents antibody binding at the cell surface, but also reduces the overall penetrability of both large and small molecules. Future studies can fine-tune the coating to determine the optimal permeability, allowing sufficient diffusion of small molecules and growth factors while preventing larger macromolecules such as antibodies and cytokines that could negatively impact cell behavior and survival. These results emphasize the comprehensive protective capabilities of the silk nanocoating in enhancing cellular resilience against various molecular intrusions.

Immune Shield Against Cytokines

The efficacy of silk nanocoatings in protecting HIOs from immune system detection and response was evaluated using Tumor Necrosis Factor alpha (TNF-α), a potent cytokine that is

known to induce apoptosis in susceptible cell types[87,88]. TNF-α, released by macrophages post-transplantation, is particularly damaging to cells and a major cause of transplantation failure[89-91]. The binding of these inflammatory cytokines to surface receptors activates downstream cascades leading to apoptosis[92,93]. To simulate a challenging immune environment, coated HIOs were exposed to 100 ng/mL of TNF-α for 72 hours and apoptosis levels were quantified using a Caspase 3/7 assay.

The results demonstrated that silk nanocoatings significantly reduced cellular susceptibility to TNF-α-induced apoptosis (Fig. 5G). Interestingly, both the 3 and 5-bilayer groups of silk coatings increased cell viability against TNF- α compared to non-coated cells, but no significant differences were observed between the different bilayers of coating (Tukey's HSD, $p = 0.36$). This suggests that the protective effect of the coating in mitigating immunogenic responses such as proteases (Fig. 4C, D) and inflammatory cytokines (Fig. 5G) is independent of coating thickness, and as little as 3-bilayers of coating is all that is necessary in minimizing immunogenic damage to cells.

These findings highlight the potential of silk nanocoatings as both physical barriers and functional shields against biochemical stressors like inflammatory cytokines. It has been proposed that the silk coating can both physically block cytokine infiltration as well as provide binding sites to capture inflammatory cytokines, preventing their contact with cells[37,86]. Our results are consistent with previous studies demonstrating the protective effects of nanocoatings in inhibiting the binding of TNF-α to TNF-receptor 1, thereby preventing apoptosis pathways in coated cells[36,94]. This capability could be particularly valuable for therapeutic applications where HIOs or transplanted cells are exposed to hostile immune environments, suggesting that silk nanocoatings could enhance the viability and functional longevity of such cellular systems in clinical settings.

Characterization of mechanical properties of silk coatings

The mechanical properties of the silk nanocoating, including height, elasticity, and stiffness, were evaluated using atomic force microscopy (AFM) nanoindentation analysis. Topography, height, and elasticity maps of a small section of a non-coated HIO were generated using the contact mode of the AFM, highlighting the differences between the HIO surface and the substrate, as shown by the color variations on the maps (Fig. 6A-C). The topography of HIO is shown in Figure 6A, while Figures 6B and C display a sample AFM-acquired elasticity map and height profile respectively. The elasticity map (Figure 6C) illustrates elastic modulus distribution, obtained by averaging the measured values at each point on the map, across the observed area of the HIO surface. Increased average elastic modulus with additional bilayers of coating was observed as non-coated HIOs exhibited an average modulus of 55.77±8.87 kPa, while 3-bilayer coated HIOs showed 115.36±3.35 kPa, and 5-bilayer coated HIOs demonstrated 137.73±17.35 kPa (Fig. 6D). These results show a significant increase in the stiffness of HIOs after encapsulation compared to the non-encapsulated control group.

Furthermore, the elastic modulus was calculated for both non-coated and coated HIOs based on the modified Bec/Tonck model, which has been previously used to determine stiffness with coated layer thickness in different coating systems [45,95-97]. The Bec/Tonck model was refined into a two-layer model that predicts the stiffness of two thin layers on a substrate[97]. This model was further simplified to eq. 01 by considering one bilayer as a single coating layer[45]. In eq. 01, E* is the global elastic modulus of the cell-silk system, which can be measured using AFM

indentation, while a is the contact radius of the projected contact area during indentation. The parameter e is the thickness of the bilayers. E, and E_S are the elastic moduli of the bilayer and substrate, respectively.

$$E^* = EE_S \frac{\pi a^2 + 6\pi a\, e + 8e^2}{\pi^2 a^2 E + 2\pi a e(2E_S + E) + 8e^2 E_S} \qquad \text{eq.01}$$

Using eq. 01 we calculated the elastic modulus of the silk-coated cell system with the following parameters: a) Es = 55.77 kPa, the stiffness of the cell, which is measured from non-coated cells using AFM; b) E=220 kPa, the stiffness of a single silk bilayer; and c) the thickness of 3 bilayers, and 5 bilayers: e= 142 nm and 236 nm, respectively. The thickness of the silk bilayers was calculated using QCM-D analysis[44]. The calculated elastic modulus for 3 bilayers and 5 bilayers of encapsulated cells were 118.29 kPa and 142.86 kPa, respectively; both values are within the standard deviation of the measured value using the AFM nanoindentation. Additionally, this model has been used to predict the variation of elastic modulus E* as a function or thickness e, and thus to predict the elastic modulus for the composed system for unknown values of the thickness parameter e. It has been shown that the elastic modulus reaches a constant value above a specific threshold thickness, thus predicting that increasing the number of bilayers above a certain threshold will not significantly affect the overall stiffness of the system[45].

This increase in stiffness with additional layers is consistent with previous studies, which have demonstrated that increasing bilayers enhances the mechanical stiffness of the entire HIO-coating construct [95,98]. The significance of the coating stiffness and elasticity lies in their influence on the biophysical cues received by the HIO[99]. The silk coating mimics the native extracellular matrix (ECM) of tissues, providing a supportive environment that impacts cellular behavior, including proliferation, differentiation, and apoptosis[100,101]. Therefore, the ability to predict manipulate the stiffness of the coating by adjusting the number of bilayers offers valuable insights and applications for coated HIOs.

Conclusions

The current study demonstrated the successful 3- and 5-bilayer silk ionomer encapsulation of HIOs, multicellular stem cell aggregates. Besides the deposition of silk onto the cell surfaces, several other key characteristics and functionalities of the coatings were observed. Namely, preservation of cell viability, proliferation, and differentiation potential after coating indicates that this nanocoating is biocompatible and suitable for cell-based therapies. Functionally, the silk coating protected HIOs from a range of environmental stressors including UV radiation, protease cleavage, inflammatory cytokines, and antibodies. Our study confirms that three bilayers are adequate under the tested conditions; however, the increase in coating stiffness with additional layers highlights a potential for tuning these properties to meet specific needs. Future research should extend beyond five bilayers to determine if there is an optimal number of layers where mechanical advantages are matched by biological benefits, thus tailoring the application to meet specific requirements of the cellular environment or clinical objectives. Overall, this work establishes a robust approach for encapsulating larger cell aggregates. This coating technique has the potential to be adapted for other types of tissue organoids, including those derived from brain, kidney, and lung tissues, broadening its applicability across a diverse range of biomedical research and therapeutic applications. The ability to protect and manipulate the immediate

cellular environment through silk nanocoating opens new avenues for enhancing cell-based therapies, particularly during transplantation procedures.

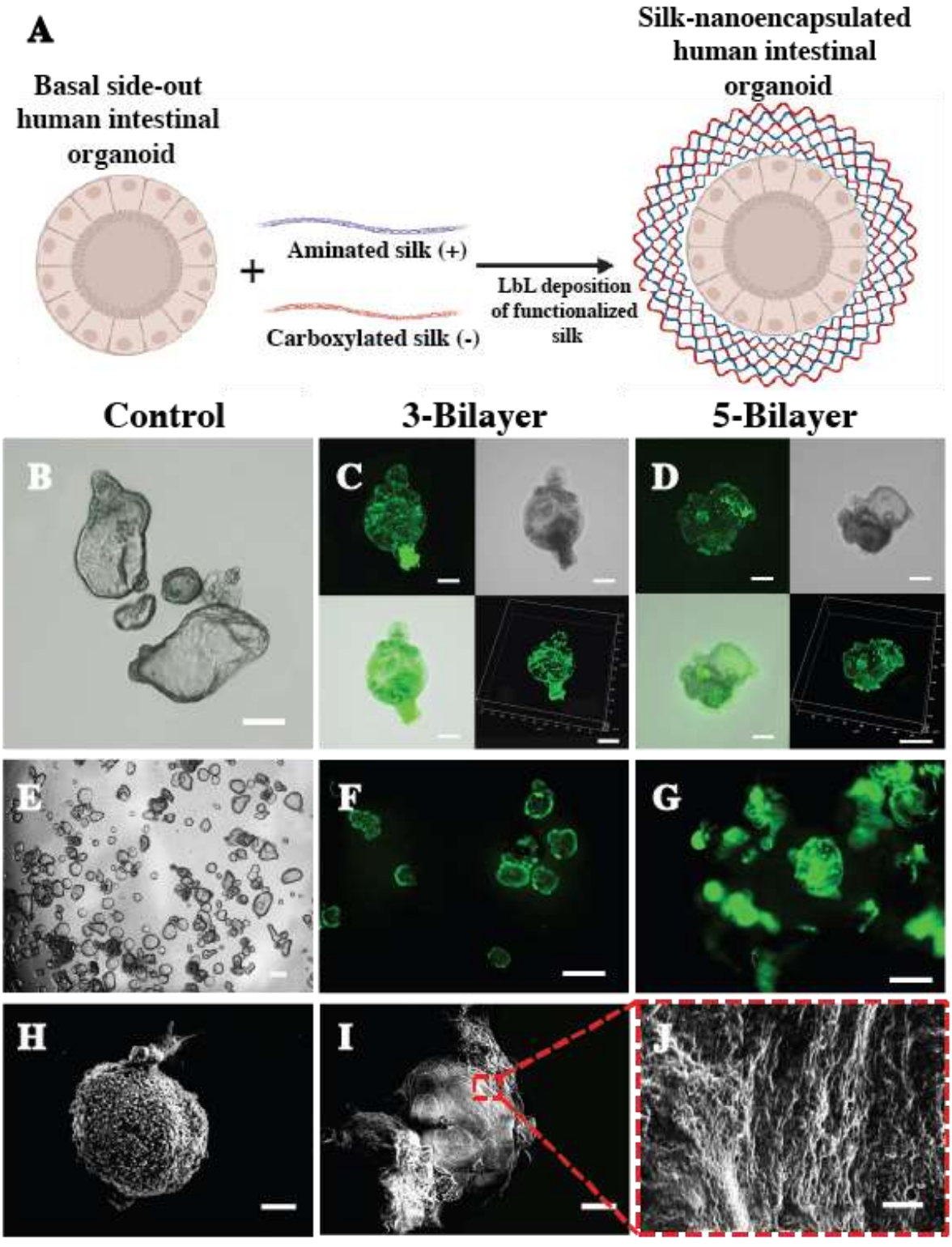

Figure 1. Successful silk deposition on HIOs visualized using FITC-labelled silk. (A) Schematic of layer-by-layer deposition of functionalized silk on human intestinal HIOs. Uncoated HIOs with characteristic cystic morphology. (B-D) 3D reconstruction via confocal imaging of uncoated HIOs, 3-bilayers coated HIOs, and 5-bilayers coated HIOs using SF-FITC. (E-G) Fluorescence microscopy of uncoated, 3-bilayer coated, and 5-bilayer coated HIOs using SF-FITC. Scale bar: 200 µm. (H) Scanning electron microscopy (SEM) imaging of an uncoated, control HIO. Scale bar: 10 µm. (I, J) SEM imaging of a 3-bilayer coated HIO at lower (scale bar: 20 µm) and higher magnifications (scale bar: 2 µm), respectively.

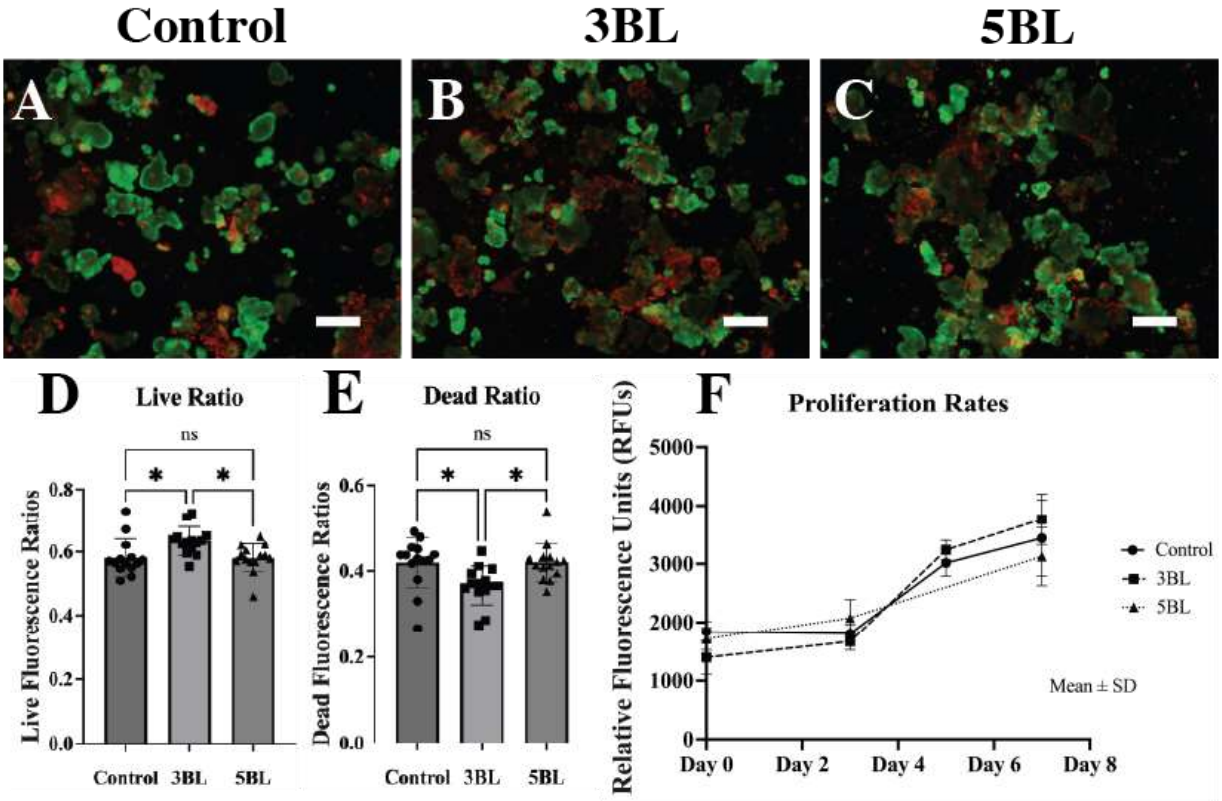

Figure 2. Cell viability and proliferation post-encapsulation with either 3 or 5 bilayers (BL) of silk. (A, B, C) Live-dead staining of HIOs directly recovered from Matrigel, immediately after 3-bilayers of encapsulation, and 5-layers of encapsulation, respectively. Red fluorescence indicates dead cells, while green fluorescence marks living cells. Scale bar: 200 µm. (D, E) Ratio of living HIOs after encapsulation and ratio of dead or dying HIOs after encapsulation. (F) Proliferation rates of HIOs for 7 days post-encapsulation measured by AlamarBlue cell proliferation assay.

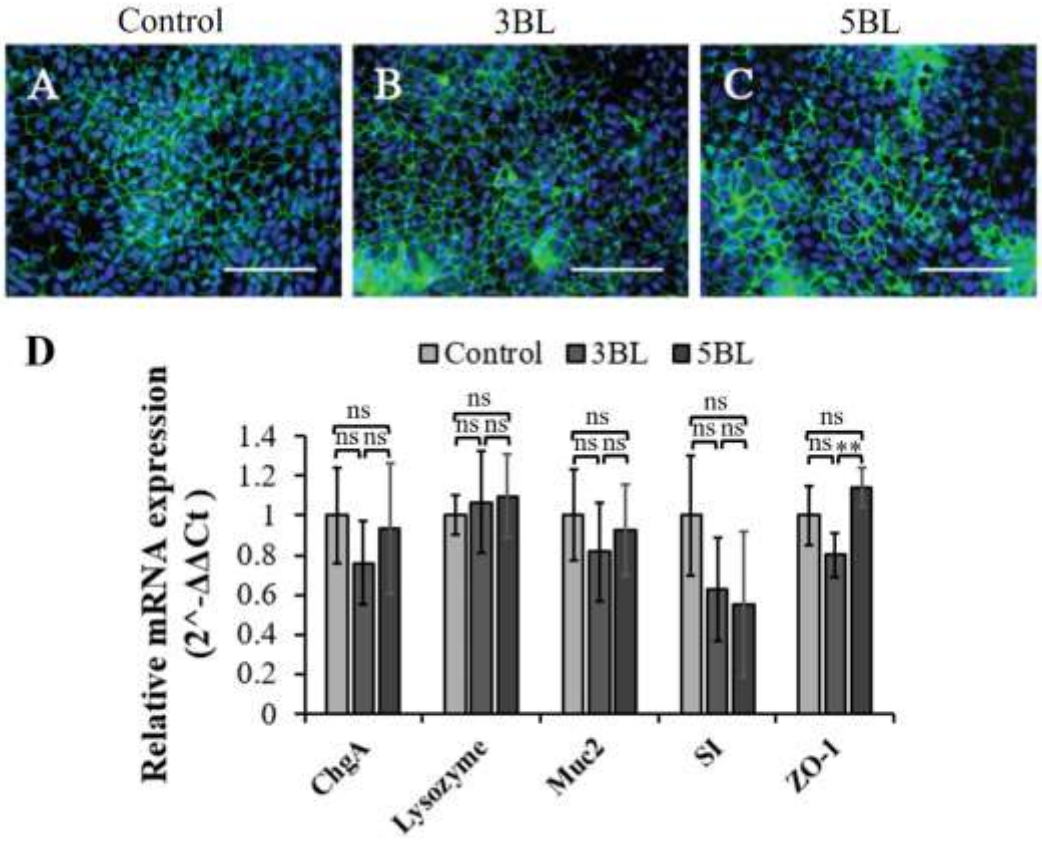

Figure 3. Differentiation potential of HIOs post-encapsulation. (A) Non-coated HIOs seeded as monolayers and immunostained with DAPI and ZO-1. (B, C) 3-layer and 5-layer coated HIOs, respectively, after coating followed by monolayer formation and differentiation. Blue, fluorescent stain is representative of nuclear DNA and green, fluorescent stain in the typical chicken-wire morphology is representative of tight-junction proteins after successful intestinal epithelial differentiation. Scale bars: 100 µm. (D) Relative mRNA expression levels 5 differentiation markers of intestinal HIOs (ChgA, Lysozyme, MUC2, SI, ZO-1) for non-coated and coated HIOs as determined by PCR after monolayer formation and differentiation.

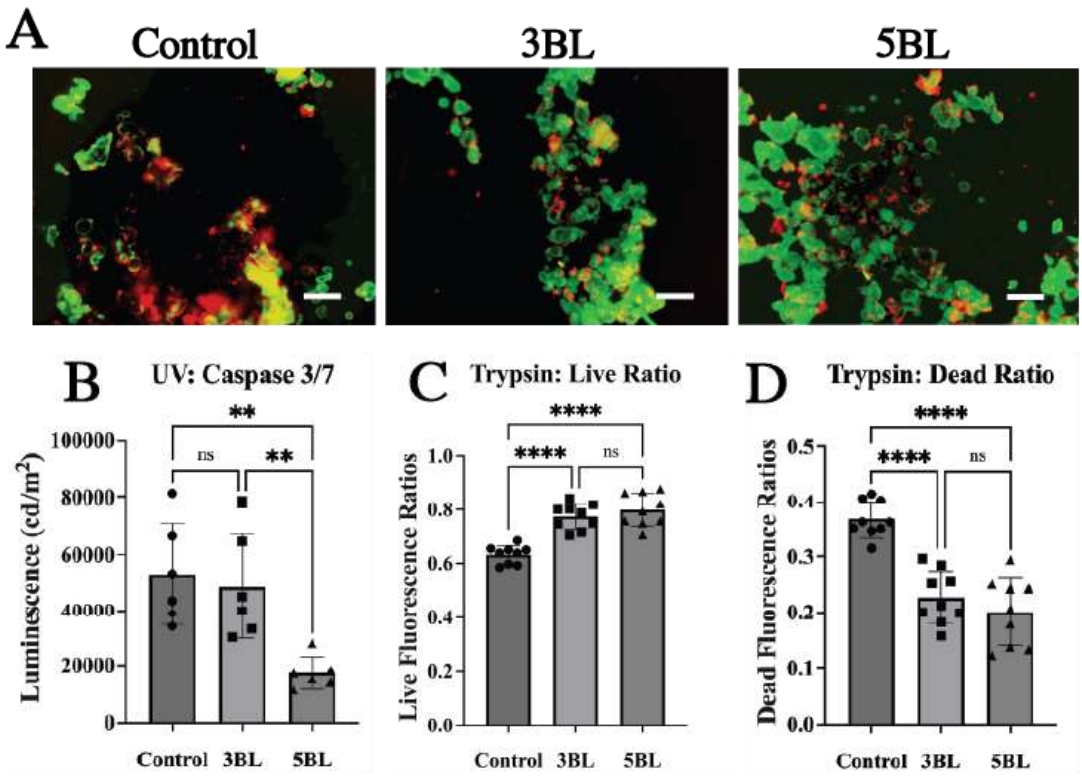

Figure 4. Functional testing of nanoencapsulation under UV-C and 0.05% trypsin conditions. (A) Caspase 3/7 assay performed after 30 minutes of UV-C treatment on non-coated and coated HIOs to determine levels of apoptosis. (B) Live-dead staining performed immediately after UV-C treatment on non-coated, 3-layer, and 5-layer coated HIOs (from top to bottom). Red-fluorescent staining shows dead cells while green-fluorescent staining shows living cells. Scale bars: 100 µm. (C, D) Live and dead ratios quantified from live-dead staining showing proportions of live and dead HIO cells after 10 minutes of exposure to 0.05% trypsin.

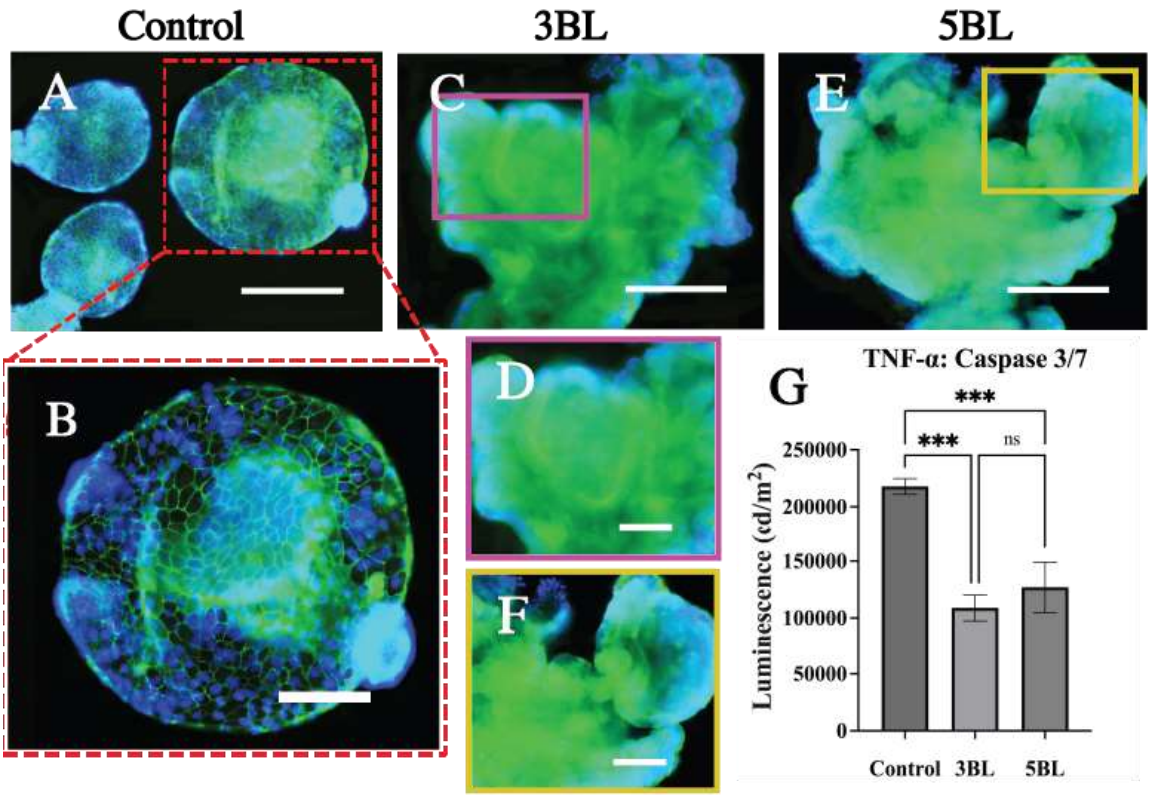

Figure 5. Functional testing of nanoencapsulation under antibody and TNF-α conditions (A, B) DAPI and ZO-1 immunostaining of non-coated HIOs at lower (Scale bars: 100 µm) and higher magnification (Scale bars: 50 µm). (C, D) DAPI and ZO-1 immunostaining of 3-bilayer coated HIOs at lower (Scale bars: 100 µm) and higher magnification (Scale bars: 50 µm. (E, F) DAPI and ZO-1 immunostaining of 5-bilayer coated HIOs at lower (Scale bars: 100 µm) and higher magnification (Scale bars: 50 µm). Note the distinct ZO-1 staining in non-coated HIOs but lack of clear ZO-1 staining in coated HIOs. (G) Caspase 3/7 assay performed on non-coated and coated HIOs after 72 hours in 100 mg/mL of TNF- α cytokine solution.

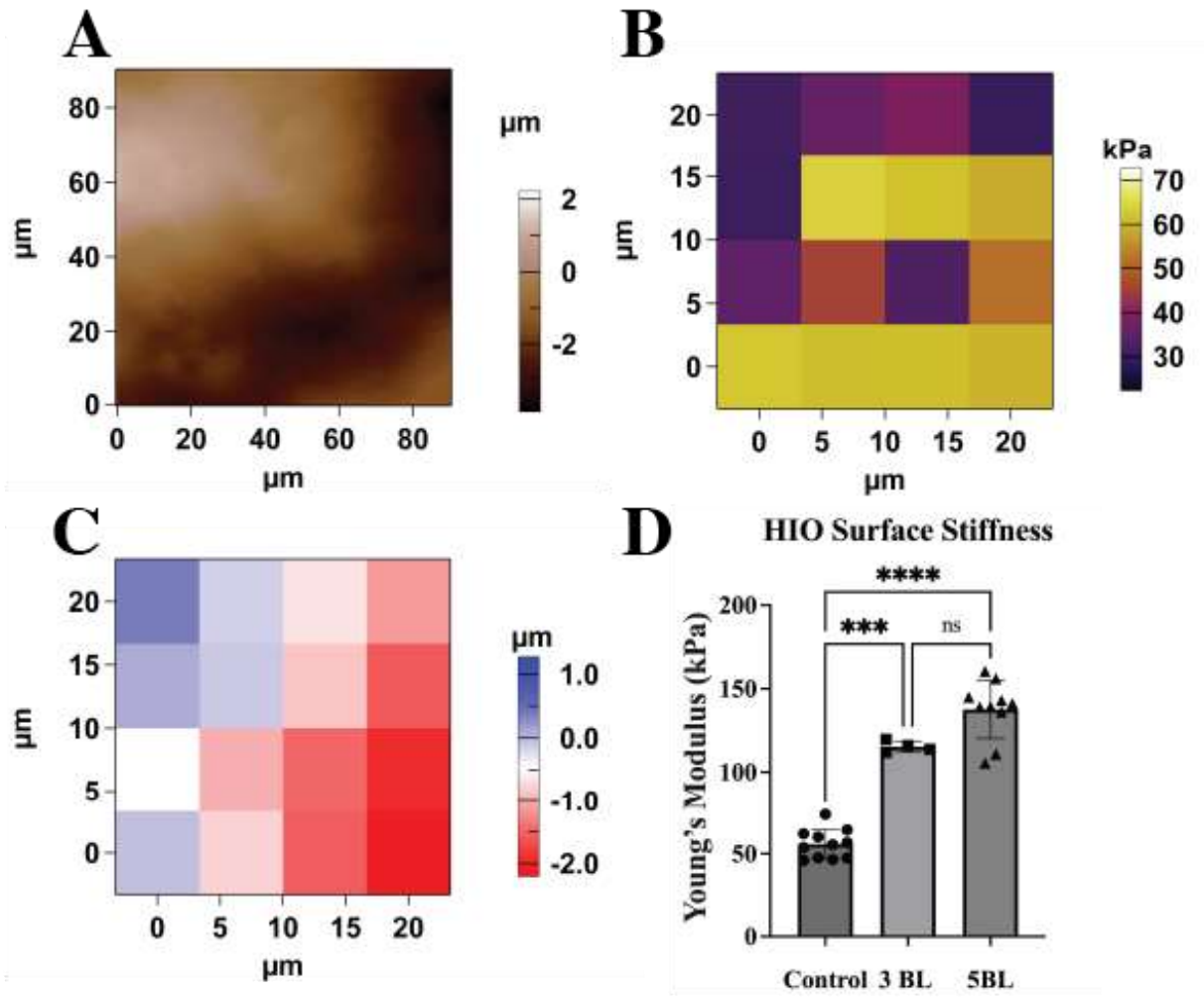

Figure 6. Mechanical characterization of HIOs using atomic force microscopy (AFM). (A) Topography map of a small surface (400 μm^2) of an uncoated HIO using the contact mode of the AFM. (B, C) Height distribution and elasticity maps, respectively, of the same HIO surface as (A). (D) HIO surface stiffness measured between the control, 3-bilayer, and 5-bilayer coated groups.

References

1 Shanks, N., Greek, R. & Greek, J. Are animal models predictive for humans? *Philos Ethics Humanit Med* **4**, 2 (2009). https://doi.org/10.1186/1747-5341-4-2

2 Greek, R. in *A Guide to the Scientific Career* 281-293 (2019).

3 Seok, J. *et al.* Genomic responses in mouse models poorly mimic human inflammatory diseases. *Proc Natl Acad Sci U S A* **110**, 3507-3512 (2013). https://doi.org/10.1073/pnas.1222878110

4 Zhao, Z. *et al.* Organoids. *Nat Rev Methods Primers* **2** (2022). https://doi.org/10.1038/s43586-022-00174-y

5 Corro, C., Novellasdemunt, L. & Li, V. S. W. A brief history of organoids. *Am J Physiol Cell Physiol* **319**, C151-C165 (2020). https://doi.org/10.1152/ajpcell.00120.2020

6 Yang, S. *et al.* Organoids: The current status and biomedical applications. *MedComm (2020)* **4**, e274 (2023). https://doi.org/10.1002/mco2.274

7 Rahmani, S., Breyner, N. M., Su, H. M., Verdu, E. F. & Didar, T. F. Intestinal organoids: A new paradigm for engineering intestinal epithelium in vitro. *Biomaterials* **194**, 195-214 (2019). https://doi.org/10.1016/j.biomaterials.2018.12.006

8 Puschhof, J., Pleguezuelos-Manzano, C. & Clevers, H. Organoids and organs-on-chips: Insights into human gut-microbe interactions. *Cell Host Microbe* **29**, 867-878 (2021). https://doi.org/10.1016/j.chom.2021.04.002

9 Co, J. Y., Margalef-Català, M., Monack, D. M. & Amieva, M. R. Controlling the polarity of human gastrointestinal organoids to investigate epithelial biology and infectious diseases. *Nature Protocols* **16**, 5171-5192 (2021). https://doi.org/10.1038/s41596-021-00607-0

10 Saxena, K. *et al.* Human Intestinal Enteroids: a New Model To Study Human Rotavirus Infection, Host Restriction, and Pathophysiology. *J Virol* **90**, 43-56 (2016). https://doi.org/10.1128/JVI.01930-15

11 Forbester Jessica, L. *et al.* Interaction of Salmonella enterica Serovar Typhimurium with Intestinal Organoids Derived from Human Induced Pluripotent Stem Cells. *Infection and Immunity* **83**, 2926-2934 (2015). https://doi.org/10.1128/iai.00161-15

12 Niklinska-Schirtz, B. J. *et al.* Ileal Derived Organoids From Crohn's Disease Patients Show Unique Transcriptomic and Secretomic Signatures. *Cell Mol Gastroenterol Hepatol* **12**, 1267-1280 (2021). https://doi.org/10.1016/j.jcmgh.2021.06.018

13 Sarvestani, S. K. *et al.* Induced organoids derived from patients with ulcerative colitis recapitulate colitic reactivity. *Nature Communications* **12**, 262 (2021). https://doi.org/10.1038/s41467-020-20351-5

14 Drost, J. & Clevers, H. Organoids in cancer research. *Nature Reviews Cancer* **18**, 407-418 (2018). https://doi.org/10.1038/s41568-018-0007-6

15 Drost, J. *et al.* Sequential cancer mutations in cultured human intestinal stem cells. *Nature* **521**, 43-47 (2015). https://doi.org/10.1038/nature14415

16 Vlachogiannis, G. *et al.* Patient-derived organoids model treatment response of metastatic gastrointestinal cancers. *Science* **359**, 920-926 (2018). https://doi.org/10.1126/science.aao2774

17 Singh, A. *et al.* Transplanted human intestinal organoids: a resource for modeling human intestinal development. *Development* **150** (2023). https://doi.org/10.1242/dev.201416
18 Flood, P., Hanrahan, N., Nally, K. & Melgar, S. Human intestinal organoids: Modeling gastrointestinal physiology and immunopathology — current applications and limitations. *European Journal of Immunology* **54**, 2250248 (2024). https://doi.org/https://doi.org/10.1002/eji.202250248
19 Choi, W. H., Bae, D. H. & Yoo, J. Current status and prospects of organoid-based regenerative medicine. *BMB Rep* **56**, 10-14 (2023). https://doi.org/10.5483/BMBRep.2022-0195
20 Sagrac, D. *et al.* Organoids in Tissue Transplantation. *Adv Exp Med Biol* **1347**, 45-64 (2021). https://doi.org/10.1007/5584_2021_647
21 Matsuzawa, A., Matsusaki, M. & Akashi, M. Effectiveness of nanometer-sized extracellular matrix layer-by-layer assembled films for a cell membrane coating protecting cells from physical stress. *Langmuir* **29**, 7362-7368 (2013). https://doi.org/10.1021/la303459v
22 Hasturk, O. *et al.* Silk nanocoatings of mammalian cells for cytoprotection against mechanical stress. *Mrs Bull* **46**, 795-806 (2021). https://doi.org/10.1557/s43577-021-00114-3
23 Lee, J. *et al.* Chemical sporulation and germination: cytoprotective nanocoating of individual mammalian cells with a degradable tannic acid-FeIII complex. *Nanoscale* **7**, 18918-18922 (2015). https://doi.org/10.1039/c5nr05573c
24 Shi, P., Zhao, N., Coyne, J. & Wang, Y. DNA-templated synthesis of biomimetic cell wall for nanoencapsulation and protection of mammalian cells. *Nature Communications* **10**, 2223 (2019). https://doi.org/10.1038/s41467-019-10231-y
25 Youn, W. *et al.* Cytoprotective Encapsulation of Individual Jurkat T Cells within Durable TiO(2) Shells for T-Cell Therapy. *Angew Chem Int Ed Engl* **56**, 10702-10706 (2017). https://doi.org/10.1002/anie.201703886
26 Zhao, Z. *et al.* Nanocaged enzymes with enhanced catalytic activity and increased stability against protease digestion. *Nat Commun* **7**, 10619 (2016). https://doi.org/10.1038/ncomms10619
27 de Groot, M. *et al.* Microcapsules and their ability to protect islets against cytokine-mediated dysfunction. *Transplantation Proceedings* **33**, 1711-1712 (2001). https://doi.org/https://doi.org/10.1016/S0041-1345(00)02653-1
28 Olabisi, R. M. Cell microencapsulation with synthetic polymers. *J Biomed Mater Res A* **103**, 846-859 (2015). https://doi.org/10.1002/jbm.a.35205
29 Orive, G. *et al.* Cell encapsulation: promise and progress. *Nat Med* **9**, 104-107 (2003). https://doi.org/10.1038/nm0103-104
30 Schmidt, J. J., Rowley, J. & Kong, H. J. Hydrogels used for cell-based drug delivery. *J Biomed Mater Res A* **87**, 1113-1122 (2008). https://doi.org/10.1002/jbm.a.32287
31 De, S. & Robinson, D. Polymer relationships during preparation of chitosan-alginate and poly-l-lysine-alginate nanospheres. *J Control Release* **89**, 101-112 (2003). https://doi.org/10.1016/s0168-3659(03)00098-1

32 Park, J. H. *et al.* Nanocoating of single cells: from maintenance of cell viability to manipulation of cellular activities. *Adv Mater* **26**, 2001-2010 (2014). https://doi.org/10.1002/adma.201304568
33 Xue, Z., Mei, D. & Zhang, L. Advances in single-cell nanoencapsulation and applications in diseases. *J Microencapsul* **39**, 481-494 (2022). https://doi.org/10.1080/02652048.2022.2111472
34 De Vos, P., De Haan, B. & Van Schilfgaarde, R. Effect of the alginate composition on the biocompatibility of alginate-polylysine microcapsules. *Biomaterials* **18**, 273-278 (1997). https://doi.org/10.1016/s0142-9612(96)00135-4
35 Ponce, S. *et al.* Chemistry and the biological response against immunoisolating alginate-polycation capsules of different composition. *Biomaterials* **27**, 4831-4839 (2006). https://doi.org/10.1016/j.biomaterials.2006.05.014
36 Li, W. *et al.* Manipulable Permeability of Nanogel Encapsulation on Cells Exerts Protective Effect against TNF-alpha-Induced Apoptosis. *ACS Biomater Sci Eng* **4**, 2825-2835 (2018). https://doi.org/10.1021/acsbiomaterials.8b00654
37 Yang, J. *et al.* Nanoencapsulation of individual mammalian cells with cytoprotective polymer shell. *Biomaterials* **133**, 253-262 (2017). https://doi.org/10.1016/j.biomaterials.2017.04.020
38 Youn, W. *et al.* Single-Cell Nanoencapsulation: From Passive to Active Shells. *Adv Mater* **32**, e1907001 (2020). https://doi.org/10.1002/adma.201907001
39 Hwang, J. *et al.* Synthesis and Characterization of Functional Nanofilm-Coated Live Immune Cells. *ACS Appl Mater Interfaces* **10**, 17685-17692 (2018). https://doi.org/10.1021/acsami.8b04275
40 Zhang, C. *et al.* Supramolecular Nanofibers Containing Arginine-Glycine-Aspartate (RGD) Peptides Boost Therapeutic Efficacy of Extracellular Vesicles in Kidney Repair. *ACS Nano* **14**, 12133-12147 (2020). https://doi.org/10.1021/acsnano.0c05681
41 Li, W. *et al.* The Effect of Layer-by-Layer Assembly Coating on the Proliferation and Differentiation of Neural Stem Cells. *ACS Appl Mater Interfaces* **7**, 3018-3029 (2015). https://doi.org/10.1021/am504456t
42 Silva, J. M., Garcia, J. R., Reis, R. L., Garcia, A. J. & Mano, J. F. Tuning cell adhesive properties via layer-by-layer assembly of chitosan and alginate. *Acta Biomater* **51**, 279-293 (2017). https://doi.org/10.1016/j.actbio.2017.01.058
43 Zhi, Z. L., Liu, B., Jones, P. M. & Pickup, J. C. Polysaccharide multilayer nanoencapsulation of insulin-producing beta-cells grown as pseudoislets for potential cellular delivery of insulin. *Biomacromolecules* **11**, 610-616 (2010). https://doi.org/10.1021/bm901152k
44 Hasturk, O., Sahoo, J. K. & Kaplan, D. L. Synthesis and Characterization of Silk Ionomers for Layer-by-Layer Electrostatic Deposition on Individual Mammalian Cells. *Biomacromolecules* **21**, 2829-2843 (2020). https://doi.org/10.1021/acs.biomac.0c00523
45 Kumarasinghe, U. *et al.* Impact of Silk-Ionomer Encapsulation on Immune Cell Mechanical Properties and Viability. *ACS Biomaterials Science & Engineering* (2024). https://doi.org/10.1021/acsbiomaterials.4c00412
46 Rockwood, D. N. *et al.* Materials fabrication from Bombyx mori silk fibroin. *Nat Protoc* **6**, 1612-1631 (2011). https://doi.org/10.1038/nprot.2011.379

47 Vepari, C. & Kaplan, D. L. Silk as a Biomaterial. *Prog Polym Sci* **32**, 991-1007 (2007). https://doi.org/10.1016/j.progpolymsci.2007.05.013
48 Drachuk, I. *et al.* Silk macromolecules with amino acid-poly(ethylene glycol) grafts for controlling layer-by-layer encapsulation and aggregation of recombinant bacterial cells. *ACS Nano* **9**, 1219-1235 (2015). https://doi.org/10.1021/nn504890z
49 Drachuk, I. *et al.* Cell surface engineering with edible protein nanoshells. *Small* **9**, 3128-3137 (2013). https://doi.org/10.1002/smll.201202992
50 Mansouri, S., Merhi, Y., Winnik, F. M. & Tabrizian, M. Investigation of layer-by-layer assembly of polyelectrolytes on fully functional human red blood cells in suspension for attenuated immune response. *Biomacromolecules* **12**, 585-592 (2011). https://doi.org/10.1021/bm101200c
51 Chen, Y., Zhou, W., Roh, T., Estes, M. K. & Kaplan, D. L. In vitro enteroid-derived three-dimensional tissue model of human small intestinal epithelium with innate immune responses. *PLoS One* **12**, e0187880 (2017). https://doi.org/10.1371/journal.pone.0187880
52 Okoro, U., John, D. N. O. & Anthony, A. A. in *Application of Nanotechnology in Drug Delivery* (ed Sezer Ali Demir) Ch. 6 (IntechOpen, 2014).
53 Kumarasinghe, U. *et al.* Impact of Silk-Ionomer Encapsulation on Immune Cell Mechanical Properties and Viability. *ACS Biomater Sci Eng* **10**, 4311-4322 (2024). https://doi.org/10.1021/acsbiomaterials.4c00412
54 Fischer, D., Li, Y., Ahlemeyer, B., Krieglstein, J. & Kissel, T. In vitro cytotoxicity testing of polycations: influence of polymer structure on cell viability and hemolysis. *Biomaterials* **24**, 1121-1131 (2003). https://doi.org/https://doi.org/10.1016/S0142-9612(02)00445-3
55 Sun, J. *et al.* Transglutaminase-Catalyzed Encapsulation of Individual Mammalian Cells with Biocompatible and Cytoprotective Gelatin Nanoshells. *ACS Biomaterials Science & Engineering* **6**, 2336-2345 (2020). https://doi.org/10.1021/acsbiomaterials.0c00044
56 Yang, J. *et al.* Single mammalian cell encapsulation by in situ polymerization. *Journal of Materials Chemistry B* **4**, 7662-7668 (2016). https://doi.org/10.1039/C6TB02491B
57 Whitewolf, J. & Highley, C. B. Conformal encapsulation of mammalian stem cells using modified hyaluronic acid. *J Mater Chem B* (2024). https://doi.org/10.1039/d4tb00223g
58 Takahashi, T., Fujishima, K. & Kengaku, M. Modeling Intestinal Stem Cell Function with Organoids. *Int J Mol Sci* **22** (2021). https://doi.org/10.3390/ijms222010912
59 Meneses, A. M. C. *et al.* Intestinal Organoids-Current and Future Applications. *Vet Sci* **3** (2016). https://doi.org/10.3390/vetsci3040031
60 Wattanakull, P., Killingsworth, M. C. & Pissuwan, D. Biological responses of T cells encapsulated with polyelectrolyte-coated gold nanorods and their cellular activities in a co-culture system. *Applied Nanoscience* **7**, 667-679 (2017). https://doi.org/10.1007/s13204-017-0605-8
61 Ye, C. *et al.* Permeability and Micromechanical Properties of Silk Ionomer Microcapsules. *Langmuir* **28**, 12235-12244 (2012). https://doi.org/10.1021/la302455y
62 Geryak, R. *et al.* Tunable Interfacial Properties in Silk Ionomer Microcapsules with Tailored Multilayer Interactions. *Macromol Biosci* **19**, e1800176 (2019). https://doi.org/10.1002/mabi.201800176

63 Chen, Y. *et al.* Bioengineered 3D Tissue Model of Intestine Epithelium with Oxygen Gradients to Sustain Human Gut Microbiome. *Adv Healthc Mater* **11**, e2200447 (2022). https://doi.org/10.1002/adhm.202200447

64 Pleguezuelos-Manzano, C. *et al.* Establishment and Culture of Human Intestinal Organoids Derived from Adult Stem Cells. *Curr Protoc Immunol* **130**, e106 (2020). https://doi.org/10.1002/cpim.106

65 Gunther, C., Winner, B., Neurath, M. F. & Stappenbeck, T. S. Organoids in gastrointestinal diseases: from experimental models to clinical translation. *Gut* **71**, 1892-1908 (2022). https://doi.org/10.1136/gutjnl-2021-326560

66 Kim, J., Koo, B. K. & Knoblich, J. A. Human organoids: model systems for human biology and medicine. *Nat Rev Mol Cell Biol* **21**, 571-584 (2020). https://doi.org/10.1038/s41580-020-0259-3

67 Kobayashi, T. & Hibi, T. Improving IBD outcomes in the era of many treatment options. *Nat Rev Gastroenterol Hepatol* **20**, 79-80 (2023). https://doi.org/10.1038/s41575-022-00738-z

68 Choi, D. *et al.* Multifunctional Collagen and Hyaluronic Acid Multilayer Films on Live Mesenchymal Stem Cells. *ACS Applied Materials & Interfaces* **9**, 12264-12271 (2017). https://doi.org/10.1021/acsami.7b00365

69 Lee, H. *et al.* A Decade of Advances in Single-Cell Nanocoating for Mammalian Cells. *Advanced Healthcare Materials* **10**, 2100347 (2021). https://doi.org/https://doi.org/10.1002/adhm.202100347

70 Hwang, J.-H. *et al.* Artificial cellular nano-environment composed of collagen-based nanofilm promotes osteogenic differentiation of mesenchymal stem cells. *Acta Biomaterialia* **86**, 247-256 (2019). https://doi.org/https://doi.org/10.1016/j.actbio.2018.12.044

71 Gribova, V. *et al.* Control of the Proliferation/Differentiation Balance in Skeletal Myoblasts by Integrin and Syndecan Targeting Peptides. *ACS Biomaterials Science & Engineering* **2**, 415-425 (2016). https://doi.org/10.1021/acsbiomaterials.5b00557

72 Kim, H. *et al.* General and Facile Coating of Single Cells via Mild Reduction. *Journal of the American Chemical Society* **140**, 1199-1202 (2018). https://doi.org/10.1021/jacs.7b08440

73 Dai, T., Vrahas, M. S., Murray, C. K. & Hamblin, M. R. Ultraviolet C irradiation: an alternative antimicrobial approach to localized infections? *Expert Rev Anti Infect Ther* **10**, 185-195 (2012). https://doi.org/10.1586/eri.11.166

74 Reed, N. G. The history of ultraviolet germicidal irradiation for air disinfection. *Public Health Rep* **125**, 15-27 (2010). https://doi.org/10.1177/003335491012500105

75 Antosiewicz, J. M. & Shugar, D. UV-Vis spectroscopy of tyrosine side-groups in studies of protein structure. Part 2: selected applications. *Biophys Rev* **8**, 163-177 (2016). https://doi.org/10.1007/s12551-016-0197-7

76 Hasturk, O. *et al.* Cytoprotection of Human Progenitor and Stem Cells through Encapsulation in Alginate Templated, Dual Crosslinked Silk and Silk-Gelatin Composite Hydrogel Microbeads. *Adv Healthc Mater* **11**, e2200293 (2022). https://doi.org/10.1002/adhm.202200293

77 Wang, B. *et al.* Guarding embryo development of zebrafish by shell engineering: a strategy to shield life from ozone depletion. *PLoS One* **5**, e9963 (2010). https://doi.org/10.1371/journal.pone.0009963

78 Antalis, T. M., Shea-Donohue, T., Vogel, S. N., Sears, C. & Fasano, A. Mechanisms of disease: protease functions in intestinal mucosal pathobiology. *Nat Clin Pract Gastroenterol Hepatol* **4**, 393-402 (2007). https://doi.org/10.1038/ncpgasthep0846

79 Choy, J. C. Granzymes and perforin in solid organ transplant rejection. *Cell Death & Differentiation* **17**, 567-576 (2010). https://doi.org/10.1038/cdd.2009.161

80 Magrassi, R., Ramoino, P., Bianchini, P. & Diaspro, A. Protection capabilities of nanostructured shells toward cell encapsulation: A saccharomyces/paramecium model. *Microscopy Research and Technique* **73**, 931-936 (2010). https://doi.org/https://doi.org/10.1002/jemt.20844

81 Yang, J., Yang, Y., Kawazoe, N. & Chen, G. Encapsulation of individual living cells with enzyme responsive polymer nanoshell. *Biomaterials* **197**, 317-326 (2019). https://doi.org/https://doi.org/10.1016/j.biomaterials.2019.01.029

82 Sharony, R. *et al.* Protein targets of inflammatory serine proteases and cardiovascular disease. *J Inflamm (Lond)* **7**, 45 (2010). https://doi.org/10.1186/1476-9255-7-45

83 Byskov, K., Le Gall, S. M., Thiede, B., Camerer, E. & Kanse, S. M. Protease activated receptors (PAR)-1 and -2 mediate cellular effects of factor VII activating protease (FSAP). *The FASEB Journal* **34**, 1079-1090 (2020). https://doi.org/https://doi.org/10.1096/fj.201801986RR

84 Valenzuela, N. M. & Reed, E. F. Antibodies in transplantation: the effects of HLA and non-HLA antibody binding and mechanisms of injury. *Methods Mol Biol* **1034**, 41-70 (2013). https://doi.org/10.1007/978-1-62703-493-7_2

85 Chelakkot, C., Ghim, J. & Ryu, S. H. Mechanisms regulating intestinal barrier integrity and its pathological implications. *Experimental & Molecular Medicine* **50**, 1-9 (2018). https://doi.org/10.1038/s12276-018-0126-x

86 Krol, S. *et al.* Multilayer Nanoencapsulation. New Approach for Immune Protection of Human Pancreatic Islets. *Nano Letters* **6**, 1933-1939 (2006). https://doi.org/10.1021/nl061049r

87 Rath, P. C. & Aggarwal, B. B. TNF-induced signaling in apoptosis. *J Clin Immunol* **19**, 350-364 (1999). https://doi.org/10.1023/a:1020546615229

88 Webster, J. D. & Vucic, D. The Balance of TNF Mediated Pathways Regulates Inflammatory Cell Death Signaling in Healthy and Diseased Tissues. *Frontiers in Cell and Developmental Biology* **8** (2020). https://doi.org/10.3389/fcell.2020.00365

89 Kale, A. & Rogers, N. M. No Time to Die-How Islets Meet Their Demise in Transplantation. *Cells* **12** (2023). https://doi.org/10.3390/cells12050796

90 Parameswaran, N. & Patial, S. Tumor necrosis factor-α signaling in macrophages. *Crit Rev Eukaryot Gene Expr* **20**, 87-103 (2010). https://doi.org/10.1615/critreveukargeneexpr.v20.i2.10

91 Jaber, F. L., Sharma, Y., Mui, B. G., Kapoor, S. & Gupta, S. Tumor Necrosis Factor Directs Allograft-Related Innate Responses and Its Neutralization Improves Hepatocyte Engraftment in Rats. *Am J Pathol* **191**, 79-89 (2021). https://doi.org/10.1016/j.ajpath.2020.09.014

92 Varfolomeev, E. E. & Ashkenazi, A. Tumor Necrosis Factor: An Apoptosis JuNKie? *Cell* **116**, 491-497 (2004). https://doi.org/10.1016/S0092-8674(04)00166-7
93 Wang, L., Du, F. & Wang, X. TNF-alpha induces two distinct caspase-8 activation pathways. *Cell* **133**, 693-703 (2008). https://doi.org/10.1016/j.cell.2008.03.036
94 Ashari, N. *et al.* Silk fibroin preserves beta cell function under inflammatory stress while stimulating islet cell surface GLUT2 expression. *Cell Immunol* **329**, 10-16 (2018). https://doi.org/10.1016/j.cellimm.2018.04.004
95 Menga, N., Putignano, C., Afferrante, L. & Carbone, G. The Contact Mechanics of Coated Elastic Solids: Effect of Coating Thickness and Stiffness. *Tribology Letters* **67**, 24 (2019). https://doi.org/10.1007/s11249-019-1137-z
96 Bec, S., Tonck, A. & Loubet, J. L. A simple guide to determine elastic properties of films on substrate from nanoindentation experiments. *Philosophical Magazine* **86**, 5347-5358 (2006). https://doi.org/10.1080/14786430600660856
97 Pailler-Mattei, C., Bec, S. & Zahouani, H. In vivo measurements of the elastic mechanical properties of human skin by indentation tests. *Medical Engineering & Physics* **30**, 599-606 (2008). https://doi.org/https://doi.org/10.1016/j.medengphy.2007.06.011
98 Özenler, S. *et al.* Thickness Gradient in Polymer Coating by Reactive Layer-by-Layer Assembly on Solid Substrate. *ACS Omega* **8**, 37413-37420 (2023). https://doi.org/10.1021/acsomega.3c05445
99 Tortorella, I., Argentati, C., Emiliani, C., Martino, S. & Morena, F. The role of physical cues in the development of stem cell-derived organoids. *European Biophysics Journal* **51**, 105-117 (2022). https://doi.org/10.1007/s00249-021-01551-3
100 Bono, N. *et al.* Silk fibroin microgels as a platform for cell microencapsulation. *J Mater Sci Mater Med* **34**, 3 (2022). https://doi.org/10.1007/s10856-022-06706-y
101 Wang, X., Kluge, J. A., Leisk, G. G. & Kaplan, D. L. Sonication-induced gelation of silk fibroin for cell encapsulation. *Biomaterials* **29**, 1054-1064 (2008). https://doi.org/10.1016/j.biomaterials.2007.11.003